Egypt. J. Chem. **Vol. 66**, No. 10 pp. 443 - 456 (2023)

Egyptian Journal of Chemistry

http://ejchem.journals.ekb.eg/

Organometallic Ester Compounds as a Promising Source of New Antimicrobial Drugs

Abdou S. El-Tabla[a], Reham.M.W.Faried[a], Mohammed H. H. Abu-Setta[*a], Ahmed M.Ashour[a], Nora F.A. El-Afify[a] and Hany A. Batakoushy[b]

[1]Department of Chemistry, Faculty of Science, Menoufia University, Shebin El -Kom, Egypt
[2]Department of Pharmaceutical Analytical Chemistry, Faculty of Pharmacy, Menoufia University, Shebin Elkom, Egypt

Abstract

Mono organometallic compounds of Cu(II), Mn(II), Pb(II), Zn(II), Cd(II), Co(II), Ni(II) and Mg(II) of new diethyl 3-((2-aminophenyl)carbamoyl)-3-hydroxypentanedioate ligand have been synthesized and characterized using spectral analyses; (^{1}H-NMR, mass, IR, UV-VIS and ESR) , magnetic moments , conductance, elemental and thermal analysis. Amide ligand metal complex exhibit fluorescent properties. This approach relied on measurement the native fluorescence of the prepared ligand and its metal complexes**.** The emitted fluorescence was measured at 580 nm after excitation at 415 nm. The fluorescent intensity was proportional to different concentrations of the obtained Cu(II) complex **(4)** in the linear range of (3.0×10^{-6} to 2.9×10^{-4}). Molar conductances in DMF solutions indicated that, the complexes are non-electrolytes. The ESR spectra of solid Cu(II) complexes **(3-5)** showed an axial type symmetry indicating a $d_{(x^2-y^2)}$ ground state with a significant covalent bond character. However, Mn(II) complex **(6)**, showed an isotropic type confirming an octahedral geometry. Cytotoxic evaluation of the complexes as antimicrobial agents has been carried out; the order of inhibitory effect against Gram positive and Gram negative strains for *Streptococcus aureus was* (13)> (14,control)> (12)> (4,15)> (5)> (3,11)> (6,7)> (2,8)> (9)> (16) ,for *B. subtilis* the order of cytotoxic effect is (4)> (13)> (3,5,10) > (2,14,control)> (12)> (15)> (11)> (7)> (8)> (6)> (9,16). Furthermore for *E.coli* the order is (control > 4,13)> (14)> (5,15)> (3,12)> (10)> (11)> (2)> (6,7)> (8,9,16) and also for *protteus vulgaris* the order is (13)> (10)> (11,12,14)> (15)> control> (5)> (6)> (4,7)> (8)> (3)> (2,16)> (9).Complexes showed enhanced activity in comparison to the standard drug used.

Keywords: - Hydrazone, Complexes, Spectra, Magnetism, ESR, Cytotoxicity

1. Introduction

Metallodrugs (organometallic reagents) are pharmacologically active compounds having metal atoms, which are essential for their microbial and antitumor activities, such as anticancer [1]. Metallodrugs offer many features over purely organic compounds due to specific characteristics of coordination compounds. Their bioactivity is affected by the type of central atom, its coordination and oxidation number, type and number of the ligands, coordination geometry and charge of the complex [1]. In recent years, the coordinated Chemistry of diamines have attracted the attention of researchers due to their unique capability of constructing complicated organic molecules using centers of metal as intermediates. For example, N-phenyl-ortho-phenylenediamine coordinated to platinum or nickel atoms transforms into imidazophenazine derivatives [2].The coexistence of hydrolizable ester group (-COO-) and amide group (-NHCO-), which are capable of establishing strong intermolecular hydrogen bond interactions, becomes fundamental to obtaining a suite of materials with tailored properties. Specifically, different polyester amides have been developed for biomedical applications such as drug delivery systems [3]. Literature survey reveals that nitrogen - and sulfur-containing compounds showed very good bioactivity, being potentially active against cancer as well as viral and fungal diseases [4,5]. The amide moiety has attracted further interest because it is widespread in natural and synthetic drugs and shows lower toxicity [6]. Bioactivity of amides can also be achieved by

*Corresponding author e-mail: dr.mohammedhosnyabusetta@gmail.com.; (Mohammed H. H. Abu-Setta).
EJCHEM use only: Received date 11 September 2022; revised date 10 February 2023; accepted date 19 February 2023
DOI: 10.21608/EJCHEM.2023.162209.6964

constructing the amide with hydroxypentanedioate [7]. In a variety of disciplines, such as environmental, inorganic, analytical chemistry, and bio-medical science, the fluorescence spectroscopy has developed into a common sensor that detects a highly useful substance. They have offered highly sensitive, selective, and accurate online and cost-effective detection of harmful ions of heavy metal, enzymes, and anions [8-11]. The purpose of the research is to prepare and spectroscopically characterized new metal complexes of amide ligand and also to develop an analytical method for quickly and economically detecting amide ligand. The Using spectrofluorimetric approach which has excellent simplicity, sensitivity, and selectivity.

2. Experiment

2.1. Materials and Instrumentation

All the reagents employed for the preparation of the ligand and its complexes were synthetic grade and used without further purification. TLC is used to confirm the purity of the compounds. C, H, N and Cl analyses were determined at the Analytical Unit of Cairo University, Egypt. Standard gravimetric methods were used to determine metal ions [10-12]. All metal complexes were dried under vacuum over P_4O_{10}. The IR spectra were measured as KBr pellets using a PerkinElmer 683 spectrophotometer (4000-400 cm^{-1}). Electronic spectra (qualitative) were recorded on a PerkinElmer 550 spectrophotometer. The conductances (10^{-3}M) of the complexes in DMF were measured at 25°C with a Bibby conduct meter type MCl. ^{1}H-NMR spectra of the ligand and its Cd (II) complex were obtained with PerkinElmer R32-90-MHz spectrophotometer using TMS as internal standard. Mass spectra were recorded using JEULJMS-AX-500 mass spectrometer provided with data system. The thermal analyses (DTA and TGA) were carried out in air on a Shimadzu DT-30 thermal analyzer from 27 to 800°C at a heating rate of 10°C per minute. All fluorescence measurements were acquired by an FS5 spectrofluorometer (Edinburgh, UK) with a 150 W xenon lamp source for excitation. Also, with 1-cm quartz cell and connected to Fluoracle® software. The slit widths were set to 2 nm and scanning speed 1000 nm/min. Magnetic susceptibilities were measured at 25°C by the Gouy method using mercuric tetrathiocyanatocobalt(II) as the magnetic susceptibility standard. Diamagnetic corrections were estimated from Pascal's constant[13]. The magnetic moments were calculated from the equation: The ESR spectra of solid complexes at room temperature were recorded using a varian E-109 spectrophotometer, DPPH was used as a standard material. The TLC of all compounds confirmed their purity.

2.2. Preparation of the ligand

Preparation of 4-ethoxy-2-(2-ethoxy-2-oxoethyl)-2-hydroxy-4-oxobutanoic acid

This compound (Scheme 1) was prepared by adding of 2-hydroxypropane-1,2,3-tricarboxylic acid (10 g, 0.05 mol), to ethanol (15.784 g, 0.34 mol) ;then adding three drops of conc H_2SO_4. The mixture was refluxed on water bath for 1 hour and then left to cool at room temperature to afford 4-ethoxy-2-(2-ethoxy-2-oxoethyl)-2-hydroxy-4-oxobutanoic acid.

Preparation of diethyl 3-((2-aminophenyl)carbomyl)-3- hydroxypentanedioate:

This copound (Scheme 1) was prepared by adding equimolar amount of 4-ethoxy-2-(2-ethoxy-2-oxoethyl)-2-hydroxy-4-oxobutanoic acid (12.92 g, 0.05 mol) to benzene-1,2-diamine (5.63 g, 0.05 mol) in 50 cm^3 of absolute ethanol. The mixture was refluxed with stirring for 3 hours. The light orange product which formed was filtrated off and washed with water, dried to give crude product. Then recrystallized from ethanol afford a pure needle shaped crystals of diethyl 3-((2-aminophenyl)carbamoyl)-3-hydroxypentanedioate.

Scheme 1: Preparation of ligand diethyl 3-((2-

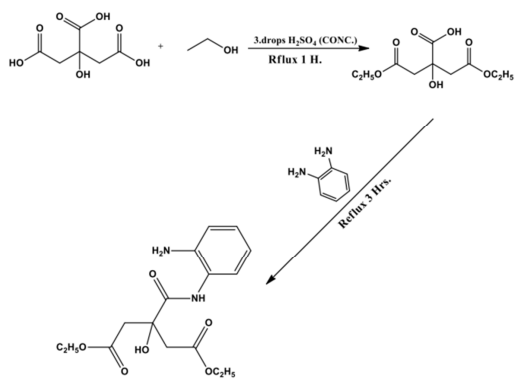

aminophenyl)carbamoyl)-3-hydroxypentanedioate

Biological activity

Antimicrobial activity

Antimicrobial activity of the metal complexes was assessed against gram positive bacteria *(Staphylcoccus aureus* and *Bacillis subtilis*), gram negative bacteria *Escherichia coli* and Proteus vulgaris) and fungi (*Aspergillus fumigates* and *Candida albicans*) by disc diffusion method. Where DMSO was used as negative control [12-14]. The bacteria were subcultured in nutrient agar medium which, composed of ($g.L^{-1}$ distilled water) NaCl (5 g), peptone (5 g), beef extract (3 g), agar (20 g). while the fungus was subcultured in

Czapek-Dox´s medium which was composed ($g.L^{-1}$ distilled water) yeast extract (1g), sucrose (30 g), $NaNO_3$, agar (20 g), KCl (0.5 g), KH_2PO_4 (1 g), $MgSO_4.7H_2O$ (0.5 g) and trace of $FeCl_3$.$6H_2O$. These media were then sterilized by autoclaving at 121 ºC for 15 min. After cooling to 45 ºC the media were poured into 90 mm diameter Petri dishes and incubated at 28 ºC. After solidify, Petri dishes were stored at 4 ºC for few hours. Microorganisms were spread over each dish by using sterile bent Loop rod. The test was performed by placing filter paper disks (3 mm diameter) with a known concentration of the compounds on the surface of the agar plates inoculated with a test organism. DMSO was used as the negative control. Standard antibacterial drug (Ampicllin (Gram positive) and Gentamicin (Gram negative). antifungal drug (Amphotricene B) and solution of metal salts were also screened under similar conditions for comparison. Plates were allowed to stand in a refrigerator for two hours before incubation to allow the tested compounds to diffuse through the agar. The Petri dishes were incubated for 48 h at 28 for fungus and at 37 for bacterium. The growth inhibition zones around the holes were observed, indicating that the examined compound inhibits the growth of microorganism. The inhibition zone was measured in millimeters carefully. All determinations were made in duplicates for each of the compounds. An average of the two independent readings for each compound was recorded.

Results and discussion

All the metal complexes are stable at room temperature, insoluble in water, not hydroscopic , partially soluble in MeOH, EtOH, $CHCl_3$ and $(CH_3)_2CO$ and completely soluble in DMF and DMSO. The analytical and physical data, spectral data (experimental part, Tables 1-2) are compatible with the proposed structures, Figures 1-4. The molar conductances of the complexes in 10^{-3} M DMF at 25 ^{o}C were in the 77.2-1.5 $ohm^{-1}cm^{2}mol^{-1}$ range, indicating a non-electrolytic nature. These low values commensurate the absence of any counters ions in their structure. Many attempts were made to grow a single crystal until now but unfortunately, they were failed. Reaction of the ligand **(1)** with metal salts using (1L: 1M) molar ratio in ethanol gave complexes **(2-16)**.

Table 1: Analytical and physical data of ligand **(1)** and its metal complexes **(2-16)**

No.	Ligand/Complexes	Color	FW	M.P (^{O}C)	Yield (%)	Anal. /Found (Calc.) (%) C	H	N	M	Conductivity Λ^{*} $*m^{-1}cm^{2}mol^{-1}$
(I)	$[H_2L]$ $C_{16}H_{26}O_8N_2$	Light orange	374.39	140	95	51.33 (51.00)	6.99 (6.80)	7.48 (7.20)	-	-
(2)	$[(H_2L)Cu(SO4)(H_2O)_2].H_2O$ $C_{16}H_{28}O_{13}CuN_2S$	Grey	552.01	285	75	34.81 (34.44)	5.11 (5.44)	5.07 (5.00)	11.51 (11.44)	9.0
(3)	$[(H_2L)Cu(H_2O)(OAc)_2].H_2O$ $C_{20}H_{32}O_{12}CuN_2$	Grey	531.98	>300	85	40.64 (40.53)	6.06 (6.77)	5.27 (5.20)	11.95 (11.66)	9.2
(4)	$[(H_2L)Cu(NO_3)_2(H_2O)].H_2O$ $C_{16}H_{26}O_{14}CuN_4$	Purple	561.94	280	71	34.19 (34.99)	4.66 (4.58)	9.97 (9.66)	11.31 (11.45)	77.2
(5)	$[(H_2L)Cu(Cl)_2(H_2O)].2H_2O$ $C_{16}H_{28}O_9CuN_2Cl_2$	Black	526.85	360	89	36.48 (36.44)	5.36 (5.22)	5.32 (5.44)	12.06 (12.66)	45.8
(6)	$[(H_2L)Mn(Cl)_2(H_2O)].2H_2O$ $C_{16}H_{28}O_9MnCl_2N_2$	Off white	518.24	>300	70	37.08 (37.77)	5.45 (5.44)	5.41 (5.66)	10.60 (10.56)	6.3
(7)	$[(H_2L)Mn(OAc)_2(H_2O)]$ $C_{20}H_{30}O_{11}MnN_2$	Orange	529.39	262	74	45.38 (45.31)	5.71 (5.53)	5.29 (5.37)	10.38 (10.28)	31.8
(8)	$[(H_2L)Pb(NO_3)_2(H_2O)].H_2O$ $C_{16}H_{26}O_{14}PbN_4$	Light brown	705.59	350	87	27.24 (27.25)	3.71 (3.66)	7.94 (7.55)	29.37 (29.55)	10.4
(9)	$[(H_2L)Pb(OAc)_2(H_2O)].2H_2O$ $C_{22}H_{34}O_{13}PbN_2$	Dark brown	717.69	>300	88	33.47 (33.24)	4.77 (4.42)	3.90 (3.64)	28.87 (28.65)	1.5
(10)	$[(H_2L)Zn(OAc)_2(H_2O)].H_2O$ $C_{20}H_{32}O_{12}ZnN_2$	Brown	557.88	259.2	82	43.06 (43.14)	5.78 (5.65)	5.02 (5.19)	11.72 (11.65)	26.6
(11)	$[(H_2L)Zn(Cl)_2(H_2O)].H_2O$ $C_{16}H_{26}O_8ZnN_2Cl_2$	Brown	510.70	251.6	65	37.63 (37.82)	5.13 (5.48)	5.49 (5.65)	12.81 (12.97)	26.8
(12)	$[(H_2L)Cd(OAc)_2(H_2O)].2H_2O$ $C_{20}H_{34}O_{13}CdN_2$	Bale brown	622.89	255	84	38.56 (38.62)	5.50 (5.32)	4.49 (4.58)	18.05 (18.12)	11.4
(13)	$[(H_2L)Cd(Cl)_2(H_2O)].H_2O$ $C_{16}H_{26}O_8CdN_2Cl_2$	Light beige	557.7	285	77	34.46 (34.17)	4.69 (4.73)	5.02 (5.48)	20.16 (20.31)	23.7
(14)	$[(H_2L)Co(OAc)_2(H_2O)].H_2O$ $C_{20}H_{32}O_{12}CoN_2$	Black	551.41	340	55	43.56 (43.45)	5.84 (5.78)	5.08 (5.10)	10.69 (10.57)	3.6
(15)	$[(H_2L)Ni(Cl)_2(H_2O)].H_2O$ $C_{16}H_{26}O_8NiN_2Cl_2$	Mint green	503.69	310	67	38.15 (38.22)	5.20 (5.25)	5.56 5.65	11.65 (11.54)	5.6
(16)	$[(H_2L)Mg(Cl)_2(H2O)].2H_2O$ $C_{16}H_{28}O_9MgN_2Cl_2$	Yellow	487.61	236	84	39.41 (39.35)	5.79 (5.65)	5.45 (5.11)	4.98 (4.66)	20.1

^{1}H-NMR spectra of the ligand (1) and complexes (9-11)

The ^{1}H-NMR spectra of ligand and complexes (**9-11**) in deutrated DMSO showed peaks consistent with the proposed structure. The ^{1}H-NMR spectrum of the ligand showed chemical shift observed as singlet at 10.1 ppm which was assigned to proton of aliphatic hydroxyl group. The chemical shift which appeared at 7.5 ppm was attributed to the proton of NH attached to (CH- of aromatic ring); (CO-NH-Ar-). However, The NH_2 proton of aromatic was observed as a singlet at 6.2 ppm. A set of signals appeared as multiples in the 6.5-6.7 ppm range, corresponding to protons of aromatic ring [15].By comparison the ^{1}HNMR of the ligand and the spectrum of the complexes (**9-11**); signal was observed as a singlet at 10.1 ppm characteristic to the O*H* group indicating that the ligand found in the protonated form. In addition, there is a significant downfield shift of the NH attached to (CH- of aromatic ring); (CO-NH-Ar-) proton signal relative to the free ligand clarified that the metal ions are coordinated to the amide nitrogen atom. This shift may be due to the formation of a coordination bond (N→M) [16,17] (Scheme 1& Figure 2).

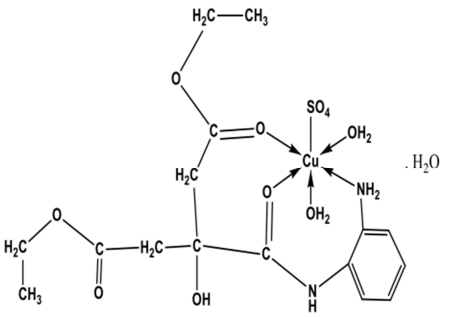

Fig. 1: Structure representation of Cu(II) complex (**2**)

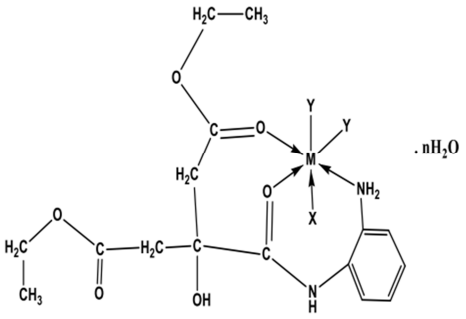

M=Cu(II)	**Y=OAc**	**X=H_2O**	**n=2**	**Complex (3)**
M=Cu(II)	**Y=NO3**	**X=H_2O**	**n=1**	**Complex (4)**
M=Cu(II)	**Y=Cl**	**X=H_2O**	**n=2**	**Complex (5)**
M=Mn(II)	**Y=Cl**	**X=H_2O**	**n=2**	**Complex (6)**
M=Mn(II)	**Y=OAc**	**X=H_2O**	**n=0**	**Complex (7)**
M=Pb(II)	**Y=NO3**	**X=H_2O**	**n=1**	**Complex (8)**
M=Pb(II)	**Y=OAc**	**X=H_2O**	**n=2**	**Complex (9)**
M=Zn(II)	**Y=OAc**	**X=H_2O**	**n=1**	**Complex (10)**

,M=Zn(II)	**Y=Cl**	**X=H_2O**	**n=1**	**Complex (11)**
,M=Cd(II)	**Y=OAc**	**X=H_2O**	**n=2**	**Complex (12)**
,M=Cd(II)	**Y=Cl**	**X=H_2O**	**n=1**	**Complex (13)**
,M=Co(II)	**Y=OAc**	**X=H_2O**	**n=1**	**Complex (14)**
,M=Ni(II)	**Y=Cl**	**X=H_2O**	**n=1**	**Complex (15)**
,M=Mg(II)	**Y=Cl**	**X=H_2O**	**n=2**	**Complex (16)**

IR spectra:

The mode of bonding between the ligand and the metal ion revealed by comparing the IR spectra of the ligand (**1**) and its metal complexes (**2**)-(**16**). The ligand showed bands in the 3620-3000 and 3000-2370 cm^{-1} ranges, commensurate the presence of two types of intra- and intermolecular hydrogen bonds of OH and NH groups with carbonyl group [18]. Thus, the higher frequency band was associated with a weaker hydrogen bond. The medium band appeared at 3100 cm^{-1} was assigned to v(NH) group [18-19]. The v(NH) group in the complexes appeared nearly at the same region of the free ligand indicating that, the NH group is not involved in the coordination to the metal ion [20]. However, the characteristic bands of v(NH_2), v(C═O) amide and v(C═O) ester were observed at (3300 and 3200), 1620 and (1900 and 1700) cm^{-1} respectively. Strong band appeared at 3400 cm^{-1} was attributed to the v(C-OH) vibration. The bands appeared at 1600,1500,830 and 740 cm^{-1} range, were assigned to v(Ar) vibration [20,21]. By comparing the IR spectra of the complexes (**2**)-(**16**) with that of the free ligand. It was found that, the position of the v(NH_2) bands were shifted by 3200,3490 cm^{-1} range towards lower wave number in the complexes indicating coordination through nitrogen of amino group (NH_2) [20,21]. The v(C═O) amide complexes appeared at 1558-1650 cm^{-1} range indicating that, the v(C═O) amide group was involved in the coordination to the metal ion [20]**.** However, the v(C═O) ester was observed at 1600-1900 cm^{-1} range towards lower wave number in the complexes indicating coordination through oxygen of carbonyl group (C═O). This is also confirmed by the appearance of new bands appeared in the 440-530 cm^{-1} range, this has been assigned to the v(M-N) [21].

In acetate complexes, (**3**), (**7**), (**9**), (**10**), (**12**), and (**14**) in these complexes bands were observed in the 820-1506 cm^{-1} range suggesting the coordination of acetate group in these complexes as a monodentate fashion [18,22].The sulphato complex (**2**) showed bands at 1243, 1170, 1076 and 707 cm^{-1} respectively assigned to monodentate sulphate group [23]. Complexes (**4**) and **(8)** show bands at 1430-820 cm^{-1} range these have been assigned to the nitrato group. Complexes (**2**)-(**16**) show bands in the 530-440 cm^{-1} was assigned to v(M-N) [22]. Complexes (**2**)-(**16**) showed bands in the 660-606 cm^{-1} range due to v(M- O) [24] . Complexes (**5**),(**6**),(**11**),(**13**),(**15**) and (**16**) showed bands in the 461-414 cm^{-1} range this has been assigned to the v(M-Cl).

Table 2: The IR Frequencies of the bands (cm^{-1}) of [H_4L] ligand (**1**) and its metal complexes

No.	ν(CH_3)	ν(CH_2)	ν(OH)	υ(H-bonding)	ν(NH)	ν(C=O) Ester	ν(NH_2)	ν(C=O) Amide	ν(Ar)	ν(OAc)/SO_4/ NO_3)	υ(M-O)	υ(M-N)	υ(M-Cl)
(1)	2900-2800	2600	3400	3620-3000 3000-2370	3100	1900,17 00	3300,32 00	1620	1600,1 500 830, 740	-	-	-	-
(2)	2740	2680	3560	3560-3180 3180-2800	3100	1750,16 35	3400,34 20	1580	1490, 760	1243,1170,10 76,707	610	515,440	-
(3)	2850	2680	3570	3600-3300 3300-2900	3150	1750,16 30	3450,34 20	1580	1490, 766	1390,1458	612	516,441	-
(4)	2870	2600	3450	3570-3290 3290-2900	3140	1750,16 50	3290,32 00	1558	1499,7 60	1350,1100,11 40,820	660	446,506	-
(5)	2940	2700	3400	3720-3000 3000-2650	3200	1700,16 30	3340,33 20	1580	1530 755	-	606	524,450	452
(6)	2900	2700	3500	3650-2940 2940-2330	3200	1700,16 40	3380,32 90	1583	1506,8 20	-	606	521	450
(7)	2900	2600	3450	3680-3170 3170-2370	3140	1640,16 25	3350,32 40	1570	1566,7 40	1502,1393	620	448,528	-
(8)	2900	2590	3450	3550-3280 3280-2500	3000	1640,16 00	3350,32 40	1570	1500,7 40	1430,1380,11 50,849	612	527,448	-
(9)	2980	2930	3530	3750-2930 2930-2500	3240	1775,17 20	3490,33 90	1650	1454,7 50	1400,1261	627	545,470	-
(10)	2900	2590	3490	3570-3250 3250-2350	3240	1700,16 40	3450,33 50	1570	1566,7 45	1503,1400	620	525,450	-
(11)	2900	2590	3500	3570-3100 3100-2450	3240	1720,16 40	3450,33 50	1566	1567,7 44	-	620	528,500	449
(12)	2890	2590	3520	3600-3000 3000-2200	3240	1700,16 40	3450,33 50	1570	1567,7 44	1503,1322	621	528,449	-
(13)	2883	2611	3450	3450-3090 3090-2500	3134	1680,16 30	3340,32 70	1570	1566,7 58	-	620	526,510	450
(14)	2950	2636	3450	3430-3050 3050-2480	3175	1705,16 44	3270,32 00	1587	1535,7 60	1506,1322	645	548,527	-
(15)	2950	2634	3400	3400-3000 3000-2500	3170	1711,16 44	3250,32 40	1589	1533,7 62	-	610	551,529	461,40
(16)	2850	2592	3565	3700-3000 3000-2240	3240	1750,16 46	3450,34 00	1565	1503,7 45	-	618	530	414

Magnetic moments:

The magnetic moments of the metal complexes (**2**)-(**16**) at room temperatures were shown in (Table 1). Cu(II) complexes (**2**)-(**5**) showed values in the 1.68-1.72 B.M, range corresponding to one unpaired electron in an octahedral structure [6,25]. Manganese(II) complexes (**6**) and (**7**) showed values 6.21 and 6.32 B.M, indicating high spin octahedral geometry around the Mn(II) ion [18,26]. Co(II) complex (**14**) showed value 4.56 B.M, indicating high spin octahedral Co(II) complex [18,26]. Ni(II) complex (**15**) showed value 3.19 B.M , indicating an octahedral Ni(II) complex [27] . Pb(II) complexes (**8-9**) , Zn(II) complex (**11**), Cd(II) complexes (**12-13**) and Mg(II) complex (**16**) showed diamagnetic property [28].

Mass spectra

The mass spectra of (**1**) and its, Cu(II) complex (**3**) Pb(II) complex **(8),** Zn(II) complex (**11**) and Cd(II) complex (**13**) confirmed their proposed formulation. The spectrum of (**1**) reveals the molecular ion peak (m/z) at 374 amu consistent with the molecular weight of the ligand. Furthermore, the fragments observed at (m/z) = 66, 122, 153, 194,247,271,293,317 and 374 amu correspond to C_3NO,$C_6H_4NO_2$, $C_7H_7NO_3$, $C_9H_8NO_4$, $C_{12}H_9NO_5$, $C_{14}H_9NO_5$, $C_{14}H_{15}NO_6$, $C_{16}H_{15}NO_6$ and $C_{16}H_{26}N_2O_8$ moieties respectively. Complex (**3**) shows fragments (m/z) at 62, 117, 214, 337.5, 423.5, 468.5, 493.5, 512.5 and 531.5 amu due to CH_4NO_2, $C_3H_5N_2O_3$, $C_7H_6N_2O_6$, $C_9H_{10}N_2O_8Cu$,

$C_{12}H_{12}N_2O_{11}Cu$, $C_{14}H_{17}N_2O_{12}Cu$, $C_{16}H_{18}N_2O_{12}Cu$, $C_{17}H_{25}N_2O_{12}Cu$ and $C_{18}H_{32}CuN_2O_{12}$ moieties respectively. The fragments observed (m⁄z) at 48,95,155,227,434,547,589,634,674 and 705 amu for complex (**8**) were assigned to CH_4O_2,CH_5NO_4, $C_2H_7N_2O_6$, $C_3H_7N_4O_8$, $C_3H_7N_4O_8Pb$, $C_7H_8N_4O_{12}Pb$, $C_9H_{10}N_4O_{13}Pb$, $C_{11}H_{15}N_4O_{14}Pb$, $C_{14}H_{19}N_4O_{14}Pb$ and $C_{16}H_{26}PbN_4O_{14}$ moieties, whereas the spectrum of Zn(II) complex (**11**) showed molecular ion peak at 510 assigned to the molecular weight of the complex and also showed fragments at 48, 100,125, 167, 272, 364, 448 which were assigned to CH_4O_2, $C_4H_4O_2$, $C_6H_5O_3$, $C_7H_5NO_4$, $C_7H_9N_2O_5Cl_2$, $C_9H_{12}N_2O_5C_{12}Zn$ and $C_{12}H_{12}N_2O_8Cl_2Zn$. However, Cd(II) complex (**13**) gave fragments (m⁄z) at 62, 76, 130, 246,358, 417, 485, 526 and 557 amu , corresponding to CH_4NO_2,$C_2H_6NO_2$,$C_4H_6N_2O_3$,$C_5H_7N_2O_5Cl_2$,$C_5H_7N_2O_5Cl_2Cd$, $C_7H_{16}N_2O_7C_{12}Cd$, $C_{11}H_{14}N_2O_8Cl_2Cd$, $C_{14}H_{19}N_2O_8Cl_2Cd$ and $C_{16}H_{26}N_2O_8Cl_2Cd$ moieties respectively.

Electronic spectra: The electronic spectral data for the ligand (**1**) and its metal complexes in DMF solution were summarized in (Table 2). Ligand (**1**) in DMF solution showed four bands at 400 nm (ε =9.65 x 10^{-3} mol^{-1} cm^{-1}), 320 nm (ε =7.72 x 10^{-3} mol^{-1} cm^{-1}), 302 nm (ε =7.28 x 10^{-3} mol^{-1} cm^{-1}) and292 nm (ε = 7.04 x 10^{-3} mol^{-1} cm^{-1}) which may be assigned to n→π* and π→π* transitions of the immine and aromatic ring respectively [29]. Cu(II) complexes **(2-5)** showed bands at 290 and 380-300 nm range , these bands were due to intraligand transitions , however, the bands appeared in the 483-425, 570-520 and 650-610 nm ranges, were assigned to O→Cu, charge transfer, $^2B^1 \rightarrow {}^2E$ and $^2B_1 \rightarrow {}^2B_2$ transitions, indicating a tetragonal octahedral structure [30,31]. However, Mn(II) complexes (**6**) and (**7**) showed bands in the 294-290, 390-300, 465-450, 585-570 ranges and 625 nm, the first bands were within the ligand and the other bands are assigned $^6A_{1g} \rightarrow {}^4E_g$, $^6A_{1g} \rightarrow {}^4T_{2g}$ and $^6A_{1g} \rightarrow {}^4T_{1g}$ transitions which were compatible to an octahedral geometry around the Mn(II) ion [26]. Pb(II) complexes (**8**) and (**9**), Zn(II) complex (**11**), Cd(II) complexes (**12**) and **(13)**, Mg(II) complex (**16**) showed bands due to intralig and transitions. Co(II) complex (**14**) showed bands at 290,395-310 range,435,578,523 and 630 nm were due to intra-ligand transitions and indicating octahedral structure which confirmed by magnetic moment is 4.56 BM [30]. However, Ni(II) complex (**15**) showed bands in the 296-290, 378-300, 465, 587, 610 and 747 nm ranges, the first three bands were within the ligand and the other bands are attributable to O→Ni charge transfer, $^3A_{2g}(F) \rightarrow {}^3T_{1g}(P)$ (ν_3), $^3A_{2g}(F) \rightarrow {}^3T_{1g}(F)$ (ν_2) and $^3A_{2g}(F) \rightarrow {}^3T_{2g}(F)$ (ν_1) transitions respectively, indicating an octahedral Ni(II) geometry [30,32]. The ν_2/ν_1 ratio for (**15**) is 1.26 which is less than the usual range of 1.5-1.75, indicating a distorted octahedral Ni(II) complex [30,33].

Table 3: Electronic spectra (nm) and magnetic moments (B.M) for the Ligand and Its complexes

No.	Ligand/Complexes	λ_{max} (nm)	μ_{eff} (BM)	ν_2/ν_1
(1)	**$[H_2L]$**	400,320,302,292	-	-
(2)	**$[(H_2L)Cu(H_2O)_2(SO_4)].H_2O$**	608,550,448,425,368,328,310,290	1.71	-
(3)	**$[(H_2L)Cu(H_2O)(OAc)_2].H_2O$**	650,570,520,455,350,323,308,290	1.69	-
(4)	**$[(H_2L)$ Cu $(NO_3)_2(H_2O)]. H_2O$**	610,530,447,430,380,310,300,290	1.68	
(5)	**$[(H_2L)$ Cu(Cl)$_2(H_2O)$].$2H_2O$**	615,483,440,374,310,300,290	1.72	
(6)	**$[(H_2LMn(H2O)Cl2].2H_2O$**	625,570,450,390,313,292	6.21`	-
(7)	**$[(H_2L)$ Mn $(OAc)_2$ (H_2O)]**	625,585,465,370,308,300,294,290	6.32	
(8)	**$[(H_2L)$ Pb $(NO_3)_2(H_2O)$]. H_2O**	390,310,306,286	Diamagnetic	
(9)	**$[(H_2L)$ Pb$(OAc)_2(H_2O)]$. $2H_2O$**	384,310,307,300,288	Diamagnetic	
(11)	**$[(H_2L)$ Zn$(Cl)_2(H_2O)$] . H_2O**	400,310,300,292	Diamagnetic	
(12)	**$[(H_2L)Cd$ $(OAc)_2(H_2O)$].$2H_2O$**	385,310,306,300,292	Diamagnetic	
(13)	**$[(H_2L)$ Cd$(Cl)_2(H_2O)]$. H_2O**	390,310,304,294,288	Diamagnetic	
(14)	**$[(H_2L)Co(H_2O)(OAc)_2]$ .H_2O**	630,578,523,435,395,370,310	4.56	1.33
(15)	**$[(H_2L)$ Ni$(Cl)_2(H_2O)]$ .H_2O**	747,610,587,465,378,310,300,290	3.19	1.26
(16)	**$[(H_2L)Mg(Cl)_2(H2O)].2H_2O$**	352,310,300,296,288	Diamagnetic	

Electron spins resonance (ESR):

The ESR spectral data for complexes **(3)-(6)** are presented in (Table 3). The spectra of Cu(II) complexes (**3-5**) are characteristic of species d^9 configuration having axial type of a $d_{(x2-y2)}$ ground state which is the most common for copper(II) complexes [18,26]. The complexes showed $g_{\|}>g^{\perp}>2.0023$, indicating octahedral geometry around copper(II) ion [34,35].The g-values are related by the expression $G = (g_{\|}-2)/ (g_{\perp} -2)$[33,34], where (G) exchange coupling interaction parameter (G). If G<4.0, a significant exchange coupling is present, whereas if G value > 4.0, local tetragonal axes are aligned parallel or only slightly misaligned. Complexes (**3**), (**4**) and (**5**) showed 3.14, 3.50 and 3.80 values indicating spin-exchange interactions toke place between copper(II) ions. This phenomena is further confirmed by the magnetic moments values (1.43 and 1.69 B.M.). On the other hand, The $g_{\|}/A_{\|}$ value is also considered as a diagnostic term for stereochemistry [36]. The $g_{\|}/A_{\|}$ values for the copper complexes are 170.77, 170.00 and 168.5 cm^{-1} which lie just within the range expected for the tetragonal distorted octahedral copper(II)complexes (Table2).

The g-value of the Cu(II) complexes with a $^2B_{1g}$ ground state ($g_{\|}>g_{\perp}$) may be expressed by [37].

$$g_{\|} = 2.002 - (8K^2_{\|}\lambda^{\circ}/\Delta E_{xy}) \quad (1)$$

$$g^{\perp} = 2.002 - (2K^2_{\perp}\lambda^{\circ}/\Delta E_{xz}) \quad (2)$$

Where $k_{\|}$ and $k_{\perp}$ are the parallel and perpendicular components respectively of the orbital reduction factor (K), λ° is the spin-orbit coupling constant for the free copper, ΔE_{xy} and ΔE_{xz} are the electron transition energies of $^2B_{1g}\rightarrow{}^2B_{2g}$ and $^2B_{1g}\rightarrow{}^2E_g$. From the above relations, the orbital reduction factors ($K_{\|}$, $K_{\perp}$, K), which are measure terms for covalency [38], can be calculated. For an ionic environment, K=1; while for a covalent environment, K<1. The lower the value of K, the greater is the covalency.

$$K^2_{\perp} = (g_{\perp}- 2.002)\,\Delta E_{xz}/2\lambda_o \quad (3)$$

$$K^2_{\|} = (g_{\|} - 2.002)\,\Delta E_{xy}/8\lambda_o \quad (4)$$

$$K^2 = (K_{2\|} + 2K^2_{\perp})/3 \quad (5)$$

K values (Table 4), for the copper(II) complexes (**3**), (**4**) and (**5**) are indicating covalent bond character [26]. Kivelson and Neiman noted that, for ionic environment $g_{\|}\geq 2.3$ and for a covalent environment $g_{\|}<2.3$ [35]. Theoretical work by Smith seems to confirm this view. The g-values reported here (Table 4) showed considerable covalent bond character [38]. Also, the in-plane σ-covalency parameter, α^2(Cu) was calculated by

$$\alpha^2\,(Cu) = (A_{\|}/0.036)+(g_{\|}-2.002)+3/7(g - 2.002)+0.04 \quad (6)$$

The calculated values (Table 2) suggested a covalent bonding [26]. The in-plane and out of- plane π-bonding coefficients β_1^2 and β^2 respectively, are dependent upon the values of ΔE_{xy} and ΔE_{xz} in the following equations [30].

$$\alpha^2\beta^2 = (g^{\perp}- 2.002)\,\Delta E_{xy}/2\lambda_o \quad (7)$$

$$\alpha^2\beta_1^2 = (g_{\|} - 2.002)\,\Delta E_{xz}/8\lambda_o \quad (8)$$

In this work, the complexes (**3**), (**4**) and (**5**) showed β_1^2 values 2.84, 2.71 and 2.41 indicating a moderate degree of covalency in the in-plane π-bonding [38].β^2 value for complexes (**3**), (**4**) and (**5**) showed 2.76,2.54 and 2.23 indicating ionic character of the out-of-plane, [26,39]. It is possible to calculate approximate orbital populations for d orbitals [40] by

$$A_{\|} = A_{iso} - 2B[1 \pm (7/4)\,\Delta g_{\|}] \quad \Delta g_{\|} = g_{\|} - g_e \quad (9)$$

$$\alpha_{p,d}^2 = 2B/\,2B^{\circ} \quad (10)$$

Where A° and 2B° is the calculated dipolar coupling for unit occupancy of d orbital respectively. When the data are analyzed, the components of the [40]. Cu hyperfine coupling were considered with all the sign combinations. The only physically meaningful results are found when $A_{\|}$ and $A_{\perp}$ were negative. The resulting isotropic coupling constant was negative and the parallel component of the dipolar coupling 2B are negative (-196.4, -183.03 and -156.00 G). These results can only occur for an orbital involving the d_{x2-y2} atomic orbital on copper. The value for 2B is quite normal for copper(Il) complexes [41]. Complex (**6**) showed isotropic spectra with g_{iso}= 2.03.

Table 4

ESR data for some metal (II) complexes

No.	$g_{\|}$	$g_{\perp}$	g_{iso} [a]	$A_{\|}$ (G)	$A_{\perp}$ (G)	A_{iso} [b] (G)	G [c]	ΔE_{xy}	ΔE_{xz}	$K_{\perp}^2$	$K_{\|}^2$	K	K^2	$g_{\|}/A_{\|}$	α^2	β^2	β_1^2	2 ß	a_d^2 (%)
(6)	-	-	2.03	-	-	-	-	-	-	-		-	-	-	-	-	-	-	-
(3)	2.22	2.07	2.12	160	10	60	3.14	16949	21505	0.69	0.71	0.83	0.70	170.77	0.25	2.76	1.84	-1.9604	83.58
(4)	2.21	2.06	2.11	150	7.5	55	3.5	16949	20833	0.59	0.65	0.78	0.61	170	0.24	2.54	1.71	183.03	77.9
(5)	2.19	2.05	2.1	130	10	50	3.8	17094	21276	0.49	0.60	0.73	0.53	168.50	0.22	2.23	1.41	156	66.40

a) $g_{iso} = (2g_{\perp} + g_{\|})/3$, **b)** $A_{iso} = (2A_{\perp} + A_{\|})/3$, **c)** $G= (g_{\|} - 2)/ (g_{\perp} - 2)$

Thermal analysis (DTA and TGA):

Since the IR spectra indicated the presence of water molecules, thermal analyses (DTA and TGA) were carried out to certain their nature. The thermal curves in the temperature 27-600°C range for complexes (**2**)-(**16**) were thermally stable up to 45 °C. Broken of hydrogen bondings occured as endothermic peak within the temperature 43-45 °C range as shown in (Table 3). Dehydration was characterized by endothermic peaks observed within the temperature 75-80°C range, corresponding to the loss of hydrated water molecules as in complexes (**2**-6) and (**8-16**). The elimination of coordinated water molecules occured in the 135-155°C range accompanied by endothermic peaks [42,43]. The TGA and DTA thermogram of Cu(II) complex (**2**) showed that, the complex decomposed in six steps. The first occurred at 43°C with no weight loss as endothermic peak, was due to break of hydrogen bondings. The second step occur at 75°C with 3.45 % weight loss (Calc. 3.26%) as endothermic peak which could be due to the elimination of hydrated water molecule. The decomposition step which occurred at 135°C with 6.89% weight loss (Calc. 6.74%) could be due to the elimination of two coordinated H_2O molecules. The TGA curve displayed another thermal decomposition at 260°C with 19.31% weight loss (Calc. 19.28%), which could be due to the loss of coordinated sulphate group. The complex showed an exothermic peak observed at 285°C was due its melting point. Finally, exothermic peaks appeared at 280, 400, 480, 500 and 610 °C corresponding to oxidative thermal decomposition which proceeded slowly with leaving CuO with 20.1% weight loss (Calc. 19.78%) [44]. The TGA and DTA thermogram of Cu(II) complex (**3**) showed endothermic peak observed at 75 with 3.45% weight loss (Calc. 3.38%) which could be due to the elimination of hydrated water molecule. The decomposition process which occurred at 150°C with 3.45% weight loss (Calc. 3.50%) could be due to the elimination of coordinated H_2O molecule. The endothermic peak observed at 240°C with 22.06% weight loss (Calc. 22.95%), could be due to the elimination of two coordinated acetate groups. Another endothermic peak observed at 315°C with no weight loss may be due to its melting point. Finally, the complex showed exothermic peaks observed at 410, 450, 530, 650 and 750°C with 20.20% weight loss (Calc. 19.97%) corresponding to oxidative thermal decomposition which proceeded slowly with final residue, assigned to CuO [33]. The TGA and DTA thermogram of Mn(II) complex (**7**) showed endothermic peak observed at 45°C, was due to break of hydrogen bondings. Another endothermic peak appeared at 155°C, with 4.45% weight loss (Calc. 4.40%), was due to loss of one coordinated water molecule. The endothermic peak observed at 240°C with 23.70% weight loss (Calc. 23.07%), could be due to the elimination of two coordinated acetate groups. Another exothermic peak observed at 262 with no weight loss may be due to its Melting point. Finally oxidative thermal decomposition occured at 440, 480, 500 and 630°C with exothermic peaks, leaving MnO with 20.50% weight loss (Calc. 20.23%) [44]. The TGA and DTA thermogram of Pb(II) complex (**8**) decomposed in six steps. The first occurred at 45°C with no weight loss as endothermic peak, was due to break of hydrogen bondings. The second step occured at 75°C with 2.76 % weight loss (Calc. 2.50%) as endothermic peak which could be due to the elimination of hydrated water molecule. Another endothermic peak observed at 150°C with 2.75% weight loss (Calc. 2.60%) was assigned to the loss of one coordinated water molecule. Another endothermic peak appeared at with 18.68% weight loss (Calc. 18.50%) was due to loss of two nitrate groups. At 350°C, endothermic peak appeared which was due to melting point. Oxidative thermal decomposition occured at 400,440,480, 500 and 620 °C with exothermic peaks, leaving PbO with 36.95% weight loss (Calc. 36.74%) [44]. The TGA and DTA thermogram of Pb(II) complex (**9**) decomposed in six steps. The first occurred at 45°C with no weight loss as endothermic peak, may be due to break of hydrogen bondings. The second step occured at 80°C with 5.02% weight loss (Calc. 4.62%) as endothermic peak which could be due to the elimination of two hydrated water molecules. Another endothermic peak observed at 150°C with 2.76% weight loss (Calc. 2.64%) was assigned to the loss of one coordinated water molecule. At 200°C, endothermic peak appeared with 17.24% weight loss (Calc. 17.78%) which was due to loss of two acetate groups. Another endothermic peak observed at with 310°C with no weight loss was due to melting point. Oxidative thermal decomposition occured at 320,350,400 and 620 °C with exothermic peaks, leaving PbO with 41.30% weight loss (Calc. 40.90%) [44]. The TGA and DTA thermogram of Zn(II) complex (**10**) decomposed in six steps. The first occurred at 45°C with no weight loss as endothermic peak, may be due to break of hydrogen bondings. The second step occured at 75°C with 3.45% weight loss (Calc. 3.23%) as endothermic peak which could be due to the elimination of hydrated water molecule. Another endothermic peak observed at 150°C with 3.45% weight loss (Calc. 3.33%) was assigned to the loss of one coordinated water molecule. Another endothermic peak at 240°C with 22.85% weight loss (Calc. 22.61%) was due to loss of two acetate groups. At 259°C, endothermic peak appeared which was due to melting point. Oxidative thermal decomposition

occured at 400,440,480, 600, 640 and 680 °C with exothermic peaks, leaving ZnO with 11.35% weight loss (Calc. 11.18%) [44] . The TGA and DTA thermogram of Cd(II) complex (**13**) showed endothermic peak at 45°C, due to break of hydrogen bonding. Another endothermic peak observed at 75°C with 3.45% weight loss (Calc. 3.23%) as endothermic peak which could be due to the elimination of hydrated water molecule. Another endothermic peak appeared at 150°C, with 3.44% weight loss (Calc. 3.43%), was due to loss of one coordinated water molecule. The endothermic peak observed at 200°C with 13.79 % weight loss (Calc. 13.61%), could be due to the elimination of two chloride ions. Another endothermic peak observed at 285°C with no weight loss may be due to its melting point. Finally oxidative thermal decomposition occured in the 400, 450, 500,600 and 630°C with exothermic peaks, leaving CdO with 28.63% weight loss (Calc. 28.49%) [44]. The TGA and DTA thermogram of Ni(II) complex (**15**) showed endothermic peak at 45°C, due to break of hydrogen bondings. Another endothermic peak observed at 75°C with 3.52% weight loss (Calc. 3.57%) as endothermic peak which could be due to the elimination of hydrated water molecule. Another endothermic peak appeared at 150°C, with 3.45% weight loss (Calc. 3.71%), was due to loss of one coordinated water molecule. The endothermic peak observed at 240°C with 15.17 % weight loss (Calc. 15.18%), could be due to the elimination of two chloride ions. Another endothermic peak observed at 310°C with no weight loss may be due to its melting310°C with no weight loss may be due to its melting point. Finally oxidative thermal decomposition occured in the 350, 400, 450,500 and 600°C with exothermic peaks, leaving NiO with 18.98% weight loss (Calc. 18.83%) [44]. The TGA and DTA thermogram of Mg(II) complex (**16**) showed that, the complex decomposed in six steps. The first occurred at 45°C with no weight loss as endothermic peak, may be due to break of hydrogen bondings. The second step occured at 75°C with 7.59 % weight loss (Calc. 7.38%) as endothermic peak which could be due to the elimination of two hydrated water molecules. The decomposition step which occurred at 150°C with 3.45% weight loss (Calc. 3.98%) could be due to the elimination of coordinated H_2O molecule. The TGA curve thermogram displayed another thermal decomposition at 200°C with 16.53% weight loss (Calc. 16.37%), which could be due to the loss of two chloride ions. The complex showed an endothermic peak observed at 236°C was due its melting point. Finally, exothermic peaks appeared at 250, 300, 450, 500 and 615 °C respectively corresponding to oxidative thermal decomposition which proceeded slowly with leaving MgO with 11.35% weight loss (Calc. 11.11%) [44].

Table 5: Thermal analyses for metal (II) complexes

NO.		*Temp. (°C)*	*DTA*		*TGA (Wt.loss %)*		
	Molecular formula		***Endo***	***Exo***	***Calcd.***	***Found***	***Assignment***
(2)	*$[(H_2L)Cu(SO_4)(H_2O)_2].H_2O$*	*43*	*endo*	*-*	*-*	*-*	*Broken of H-bondings*
		75	*endo*	*-*	*3.26*	*3.45*	*Loss of (H_2O) hydrated water molecule*
		135	*endo*	*-*	*6.74*	*6.89*	*Loss of ($2H_2O$) coordinated water molecules*
		260	*endo*	*-*	*19.28*	*19.31*	*Loss of sulphate group*
		285	*endo*	*-*	*-*	*-*	*Melting point*
		280,400,480,500	*-*	*exo*	*19.78*	*20.1*	*Decomposition process with the formation of CuO*
(3)	*$[(H_2L)Cu(H_2O)(OAc)_2].H_2O$*	*45*	*endo*	*-*	*-*	*-*	*Broken of H-bondings*
		75	*endo*	*-*	*3.38*	*3.45*	*Loss of (H_2O) hydrated water molecule*
		150	*endo*	*-*	*3.5*	*3.45*	*Loss of (H_2O) coordinated water molecule*
		240	*endo*	*-*	*22.95*	*22.06*	*Loss of two coordinated acetate groups*
		315	*endo*	*-*	*-*	*-*	*Melting point*
		410,450,530,650,750	*-*	*exo*	*19.97*	*20.20*	*Decomposition process with the formation of CuO*
(7)	*$[(H_2L)Mn(OAc)_2(H_2O)]$*	*45*	*endo*	*-*	*-*	*-*	*Broken of H-bondings*
		155	*endo*	*-*	*3.4*	*3.45*	*Loss of (H_2O) coordinated water molecule*
		240	*endo*	*-*	*23.07*	*23.7*	*Loss of two coordinated acetate groups*
		262	*-*	*exo*	*-*	*-*	*Melting point*
		440,480,500,630	*-*	*exo*	*20.23*	*20.5*	*Decomposition process with the formation of MnO*
(8)	*$[(H_2L)Pb(NO_3)_2(H_2O)].H_2O$*	*45*	*endo*	*-*	*-*	*-*	*Broken of H-bondings*
		75	*endo*	*-*	*2.5*	*2.76*	*Loss of (H_2O) hydrated water molecule*
		150	*endo*	*-*	*2.6*	*2.75*	*Loss of (H_2O) coordinated water molecule*
		220	*endo*	*-*	*18.5*	*18.68*	*Loss of two nitro groups*
		350	*endo*	*-*	*-*	*-*	*Melting point*
		400,440,480,500,620	*-*	*exo*	*36.75*	*36.95*	*Decomposition process with the formation of PbO*

(9)	*$[(H_2L)\ Pb(OAc)_2(H_2O)]\ .2H_2O$*	*45*	*endo*	*-*	*-*	*-*	*Broken of H-bondings*
		80	*endo*	*-*	*5.02*	*4.62*	*Loss of $(2H_2O)$ hydrated water molecules*
		150	*endo*	*-*	*2.64*	*2.76*	*Loss of (H_2O) coordinated water molecule*
		200	*endo*	*-*	*17.78*	*17.24*	*Loss of two coordinated acetate groups*
		310	*endo*	*-*	*-*	*-*	*Melting point*
		320,350,400,620	*-*	*exo*	*40.9*	*41.30*	*Decomposition process with the formation of PbO*
(10)	*$[(H_2L)\ Zn\ (OAc)_2(H_2O)].\ H_2O$*	*45*	*endo*	*-*	*-*	*-*	*Broken of H-bondings*
		75	*endo*	*-*	*3.23*	*3.45*	*Loss of (H_2O) hydrated water molecule*
		150	*endo*	*-*	*3.33*	*3.45*	*Loss of (H_2O) coordinated water molecule*
		240	*endo*	*-*	*22.61*	*22.85*	*Loss of two coordinated acetate groups*
		259	*endo*	*-*	*-*	*-*	*Melting point*
		400,440,480,600,640,680	*-*	*exo*	*11.18*	*11.35*	*Decomposition process with the formation of ZnO*
(13)	*$[(H_2L)\ Cd(Cl)_2(H_2O)]\ .\ H_2O$*	*45*	*endo*	*-*	*-*	*-*	*Broken of H-bondings*
		75	*endo*	*-*	*3.23*	*3.45*	*Loss of (H_2O) hydrated water molecule*
		150	*endo*	*-*	*3.34*	*3.44*	*Loss of (H_2O) coordinated water molecule*
		200	*endo*	*-*	*13.61*	*13.79*	*Loss of two Cl atoms*
		285	*endo*	*-*	*-*	*-*	*Melting point*
		400,450,500,600,700	*-*	*exo*	*28.49*	*28.63*	*Decomposition process with the formation of CdO*
(15)	*$[(H_2L)\ Ni(Cl)_2(H_2O)]\ .\ H_2O$*	*45*	*endo*	*-*	*-*	*-*	*Broken of H-bondings*
		75	*endo*	*-*	*3.27*	*3.52*	*Loss of (H_2O) hydrated water molecule*
		150	*endo*	*-*	*3.71*	*3.45*	*Loss of (H_2O) coordinated water molecule*
		240	*endo*	*-*	*15.18*	*15.17*	*Loss of two Cl atoms*
		310	*endo*	*-*	*-*	*-*	*Melting point*
		350,400,450,500,600	*-*	*exo*	*18.83*	*18.98*	*Decomposition process with the formation of NiO*
(16)	*$[(H_2L)Mg(Cl)_2(H_2O)].2H_2O$*	*45*	*endo*	*-*	*-*	*-*	*Broken of H-bondings*
		75	*endo*	*-*	*7.38*	*7.59*	*Loss of $(2H_2O)$ hydrated water molecules*
		150	*endo*	*-*	*3.98*	*3.45*	*Loss of (H_2O) coordinated water molecule*
		200	*endo*	*-*	*16.37*	*16.53*	*Loss of two Cl atoms*
		236	*endo*	*-*	*-*	*-*	*Melting point*
		250,300,450,500,615	*-*	*exo*	*11.11*	*11.35*	*Decomposition process with the formation of MgO*

Fluorescence spectroscopy

The emission spectra of the Cu(II) metal complex **(4)** was recorded in DMSO and were shown in **Fig. 2.** After an excitation wavelength of 415 nm, the Cu (II) metal complex **(4)** showed an emission wavelength of 580 nm, and discovered to be red shifted. Furthermore, the red shift of the emission wavelength in the case of Cu (II) may be caused by the primary amino group. Additionally, the conjugation of the ligand and metal complex resulted in an increase in fluorescence intensity. The copper; Cu(II) metal complex has fluorescent in nature, as seen by the fluorescence emission spectra (**Fig. 2).**

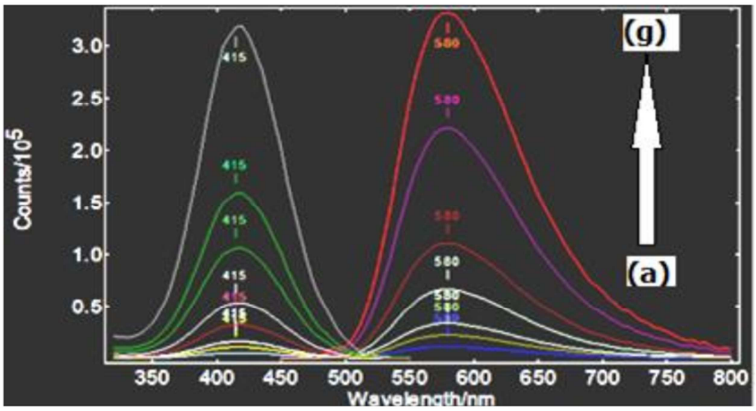

Fig. 2: Fluorescence curves of Cu(II) complex **(4)**, in DMSO at emission 580 nm after excitation at 415 nm, in concentration range (a-g, 3.0 x 10^{-6} - 2.9 x 10^{-4})

Antimicrobial activity

In vitro biological screening tests of the ligand and its metal complexes (**2-16**) were carried out as antibacterial and antifungal activity and presented in Table 5 and figure 8. The antibacterial activity was tested against two bacterial strains; Gram-positive *Streptococcus aureus* (*S. Aureus*) and *Bacillis subtilis* (*B. subtilis)* as well as Gram-negative *Escherichia coli (E.coli)* and *protteus vulgaris (P. vulgaris)* strains. The results compared with standard drug Gentamicin for Gram positive and Gram negative. The data indicated that, complexes were active against bacteria. Complexes (**2-16**) showed antibacterial activities against *Streptococcus aureus* and *Bacillis subtilis* (*B. subtilis)* [45] as well as Gram-negative *Escherichia coli (E.coli)* and *protteus vulgaris (P. vulgaris)* strains. The results showed that, the order of cytotoxic effect against Gram positive and Gram negative strains for *Streptococcus aureus is* (13)> (14),control> (12)> (4,15)> (5)> (3,11)> (6,7)> (2,8)> (9)> (16) and for *B. subtilis* the order is (4)> (13)> (3,5,10)> (2,14,control)> (12)> (15)> (11)> (7)> (8)> (6)> (9,16). Also for *E.coli* the order is (control) > (4,13)> (14)> (5,15)> (3,12)> (10)> (11)> (2)> (6,7)> (8,9,16) and also for *protteus vulgaris* the order is (13)> (10)> (11,12,14)> (15)> (control)> (5)> (6)> (4,7)> (8)> (3)> (2,16)> (9). Cu(II) complexes showed wide range of bactericidal activities against the gram positive and gram negative bacteria. The complexes were also subjected to antifungal activity against *Aspergillus fumigatus (A. fumigatus)* and *Candida albicans (C. albicans)*. The investigation showed that, Ni(II) complex (**15**) and Zn (II) complex (**10**) were more active against *Aspergillus fumigatus* whereas Mn(II) complexes (**6**) and Pb(II) complex (**9**) were not active against *Aspergillus fumigatus*. The complexes of diethyl3-((2-aminophenyl)carbamoyl)-3-ydroxypentanedioate are more active for microorganisms and this was also indicated that, nitrogen was a more effective antimicrobial agent. The increase in the activity of complexes as compared to the parent ligand may be due to the complex formation in which the ligand was coordinated to the central metal ion through the nitrogen of aromatic NH_2 group with the active centers of the cell constituents resulting in an interference with the cell process leading to an increased biological action. On comparing the results in general, it may be concluded that the complexes have greater inhibiting power than standard drug was used against all the microbes. The zone of inhibition was measured with respect to control.

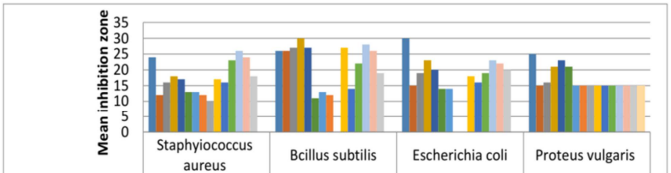

	Staphyiococcus aureus	Bcillus subtilis	Escherichia coli	Proteus vulgaris
Standard drug	24	26	30	25
Complex(2)	12	26	15	15
Complex(3)	16	27	19	16
Complex(4)	18	30	23	21
Complex(5)	17	27	20	23
Complex(6)	13	11	14	21
Complex(7)	13	13	14	15
Complex(8)	12	12	0	15
Complex(9)	10	0	0	15
Complex(10)	17	27	18	15
Complex(11)	16	14	16	15
Complex(12)	23	22	19	15
Complex(13)	26	28	23	15
Complex(14)	24	26	22	15
Complex(15)	18	19	20	15
Complex(16)	0	0	0	15

Fig.3: Biological activities of the standard drug and metal complexes (**2-16**) against bacteria

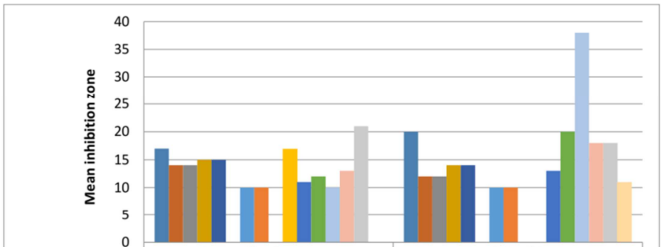

	Aspergillus fumigatus	Candida albicans
Standard drug	17	20
Complex(2)	14	12
Complex(3)	14	12
Complex(4)	15	14
Complex(5)	15	14
Complex(6)	0	0
Complex(7)	10	10
Complex(8)	10	10
Complex(9)	0	0
Complex(10)	17	0
Complex(11)	11	13
Complex(12)	12	20
Complex(13)	10	38
Complex(14)	13	18
Complex(15)	21	18
Complex(16)	0	11

Fig.4: Biological activities of the standard drug and metal complexes (**2-16**) against fungi

Conclusion

Mono organometallic complexes of Cu(II), Mn(II), Pb(II), Zn(II), Cd(II), Co(II), Ni(II) and Mg(II) ions with diethyl 3-((2-aminophenyl)carbamoyl)-3 hydroxypentanedioate ligand has much potential as antimicrobial agents. These complexes have been synthesized and characterized by (1H-NMR, mass, IR, UV-VIS, ESR) spectra, magnetic moments and conductance measurements, elemental and thermal analyses. Furthermore, copper metal complexe(4) exhibit fluorescent properties; the proposed spectrofluorimetric fluorescent method is simple, accurate, sensitive, and suitable for using the synthesized Cu(II) complex. Cytotoxic evaluation of the complexes as antimicrobial has been carried out. Complexes show enhanced activity in comparison to the standard drug used. These organometallic complexes candidates as antimicrobial agents.

References

[1]. Habala L, Pašková L, Bilková A, Bilka F, Oboňová B, Valentová J. Antimicrobial activity and cytotoxicity of transition metal carboxylates derived from agaric acid. European Pharmaceutical Journal. 2021 1;68(1):46-53.

[2]. Malkov AE, Aleksandrov GG, Ikorskii VN, Sidorov AA, Fomina IG, Nefedov SE, Novotortsev VM, Eremenko IL, Moiseev II. Reactions of ortho-phenylenediamine with a nickel trimethylacetate complex. Russian Journal of Coordination Chemistry. 2001;27(9):636-43.

[3]. Del Valle LJ, Roa M, Díaz A, Casas MT, Puiggalí J, Rodríguez-Galán A. Electrospun nanofibers of a degradable poly (ester amide). Scaffolds loaded with antimicrobial agents. Journal of Polymer Research. 2012;19(2):1-3.

[4]. Devi J, Yadav J, Lal K, Kumar N, Paul AK, Kumar D, Dutta PP, Jindal DK. Design, synthesis, crystal structure, molecular docking studies of some diorganotin (IV) complexes derived from the piperonylic hydrazide Schiff base ligands as cytotoxic agents. Journal of Molecular Structure. 2021 15;1232:129992.

[5]. Xiao Y, Bi C, Fan Y, Liu S, Zhang X, Zhang D, Wang Y, Zhu R. Synthesis, characterization and bioactivity of Schiff base copper (II) complexes derived from L-glutamine and L-asparagine. Journal of Coordination Chemistry. 2009 20;62(18):3029-39.

[6]. El Tabl A, Wahed AE, Mohamed E, Abu-Setta M. Modulation of cancer therapy using nano-organometallic compounds: preparation, spectroscopic characterization and cytotoxic evaluation. Egyptian Journal of Chemistry. 2021 1;64(7):3873-87.

[7]. Bhat M, Belagali SL, Hemanth Kumar NK, Mahadeva Kumar S. Synthesis and characterization of novel benzothiazole amide derivatives and screening as possible antimitotic and antimicrobial agents. Research on Chemical Intermediates. 2017;43(1):361-78.

[8]. Cullum BM, Vo-Dinh T. Sample collection and preparation of liquid and solids. Handbook of Spectroscopy. 2003 26;2:1.

[9]. Omar MA, Ahmed HM, Abdel Hamid MA, Batakoushy HA. New spectrofluorimetric analysis of dapagliflozin after derivatization with NBD-Cl in human plasma using factorial design experiments. Luminescence. 2019;34(6):576-84.

[10]. Omar MA, Ahmed HM, Batakoushy HA, Hamid MA. New spectrofluorimetric analysis of empagliflozin in its tablets and human plasma using two level full factorial design. Spectrochimica Acta Part A: Molecular and Biomolecular Spectroscopy. 2020 5;235:118307.

[11]. Skoog DA, Holler FJ, Crouch SR. Principles of instrumental analysis. Cengage learning; 2017 27.

[12]. Nicodemo AC, Araujo MR, Ruiz AS, Gales AC. In vitro susceptibility of Stenotrophomonas maltophilia isolates: comparison of disc diffusion, Etest and agar dilution methods. Journal of Antimicrobial Chemotherapy. 2004 1;53(4):604-8.

[13]. El-Tabl AS, Abd-El Wahed MM, Nofal ES, Saad AA. Anticancer Agents; Synthesis, Structural Characterization of Novel Di-hydrazone Ether Complexes and Study their Anticancer Activities. Journal of Chemistry and Chemical Sciences , 2018 ;8(10), 1105-1131.

[14]. McCartney JE, Collee JG, Mackie TJ. Practical medical microbiology. Charchil Livingstone; 1989.

[15]. El-Tabl AS, El-Seidy AM, Shakdofa MM, Hamdy AE. Synthesis and Spectroscopic Characterization of Copper (II), Nickel (II) and Cobalt (II) Complexes of (3, 3', 4, 4')-4, 4'-(1, 4-Phenylenbis (Azan-1-Yl-1-Ylidene)) Bis (3-(Hydroxyimino) Pentan-2-One). Smart Nanocomposites. 2011 1;2(2):111.

[16]. Maurya MR, Kumar N. Chloromethylated polystyrene cross-linked with divinylbenzene and grafted with vanadium (IV) and vanadium (V) complexes having ONO donor ligand for the catalytic activity. Journal of Molecular Catalysis A: Chemical. 2014 1;383:172-81.

[17]. Nica S, Rudolph M, Lippold I, Buchholz A, Görls H, Plass W. Vanadium (V) complex with Schiff-base ligand containing a flexible amino side chain: Synthesis, structure and reactivity. Journal of Inorganic Biochemistry. 2015 1;147:193-203.

[18]. El-Tabl AS, El-Saied FA, Al-Hakimi AN. Synthesis, spectroscopic investigation and biological activity of metal complexes with ONO trifunctionalalized hydrazone ligand. Transition Metal Chemistry. 2007;32(6):689-701.

[19]. El-Tabl AS, Shakdofa MM, El-Seidy A. Synthesis, Characterization and ESR Studies of New Copper (II) Complexes of Vicinal Oxime Ligands. Journal of the Korean Chemical Society, 2011;55(4):603-11.

[20]. Ateş D, Gulcan M, Gümüş S, Şekerci M, Özdemir S, Şahin E, Çolak N. Synthesis of bis (thiosemicarbazone) derivatives: Definition, crystal structure, biological potential and computational analysis. Phosphorus, Sulfur, and Silicon and the Related Elements. 2018 2;193(1):14-22.

[21]. El-Tabl A, Kashar T, El-Bahnasawy R, Ibrahim AE. Sythesis and characterization of novel copper (II) complexes of dehydroacetic acid thiosemicarrbazone. Polish Journal of Chemistry. 1999;73(2):245-54.

[22]. El-Tabl AS, Shakdofa MM, Herash BM. Antibacterial activities and spectroscopic characterization of synthetic metal complexes of 4-(3-(hydroxyimino)-4-oxopentan-2-ylidene) amino)-1, 5-dimethyl-2-phenyl-1H-pyrazol-3 (2H)-one. Main Group Chemistry. 2013 1;12(3):257-74.

[23]. Abdou S, Abd-El Wahed MM, Abu-Setta MH. Metallo-bioactive compounds as potential novel anticancer therapy. International Journal of Advances in Chemistry. 2018;4(1):17-37.

[24]. El-Tabl AS. Synthesis and physico-chemical studies on cobalt (II), nickel (II) and copper (II) complexes of benzidine diacetyloxime. Transition Metal Chemistry. 2002;27(2):166-70.

[25]. El-Tabl AS, Abd-El Wahed MM, El-Azm MI, Faheem SM. Newly Designed Metal-based Complexes and their Cytotoxic Effect on Hepatocellular Carcinoma, Synthesis and

Spectroscopic Studies. Journal of Chemistry and Chemical Sciences. 2020;10(1):10-31.

[26]. El-Tabl AS, Abd El-wahed MM, Abd El-Razek SE. Preparation, spectroscopic investigation and antiproliferative capacity of new metal complexes of (3E)-2-(hydroxyimino)-NP-Tolyl-3-(P-tolylimino) butanamide. Spectrochimica Acta Part A: Molecular and Biomolecular Spectroscopy. 2013 15;105:600-11.

[27]. Ramadan AE, Sawodny W, El-Baradie HY, Gaber M. Synthesis and characterization of nickel (II) complexes with symmetrical tetradentate N2O2 naphthaldimine ligands. Their application as catalysts for the hydrogenation of cyclohexene. Transition Metal Chemistry. 1997;22(3):211-5.

[28]. El-Tabl AS. Novel N, N-diacetyloximo-1, 3-phenylenediamine copper (II) complexes. Transition Metal Chemistry. 1997;22(4):400-5.

[29]. Gudasi KB, Patil MS, Vadavi RS, Shenoy RV, Patil SA, Nethaji M. X-ray crystal structure of the N-(2-hydroxy-1-naphthalidene) phenylglycine Schiff base. Synthesis and characterization of its transition metal complexes. Transition Metal Chemistry. 2006;31(5):580-5.

[30]. El-Tabl AS, El-Enein SA. Reactivity of the new potentially binucleating ligand, 2-(acetichydrazido-N-methylidene-α-naphthol)-benzothiazol, towards manganese (II), nickel (II), cobalt (II), copper (II) and zinc (II) salts. Journal of Coordination Chemistry. 2004 10;57(4):281-94.

[31]. Sallam SA, Orabi AS, El-Shetary BA, Lentz A. Copper, nickel and cobalt complexes of Schiff-bases derived from β-diketones. Transition Metal Chemistry. 2002;27(4):447-53.

[32]. Thakkar NV, Bootwala SZ. Synthesis and characterization of binuclear metal complexes derived from some isonitrosoacetophenones and benzidine 1995.

[33]. El-Tabl AS, Abd El-wahed MM, Rezk AM. Cytotoxic behavior and spectroscopic characterization of metal complexes of ethylacetoacetate bis (thiosemicarbazone) ligand. Spectrochimica Acta Part A: Molecular and Biomolecular Spectroscopy. 2014 3;117:772-88.

[34]. El-Boraey H, El-Tabl AS. Supramolecular copper (II) complexes with tetradentate ketoenamine ligands. Polish Journal of Chemistry. 2003;77(12):1759-75.

[35]. El-Tabl AS. An esr study of copper (II) complexes of N-hydroxyalkylsalicylideneimines. Transition metal chemistry. 1997;23(1):63-5.

[36]. Nikles DE, Powers MJ, Urbach FL. Copper (II) complexes with tetradentate bis (pyridyl)-dithioether and bis (pyridyl)-diamine ligands. Effect of thio ether donors on the electronic absorption spectra, redox behavior, and EPR parameters of copper (II) complexes. Inorganic Chemistry. 1983;22(22):3210-7.

[37]. Ray RK, Kauffman GB. An EPR Study of some copper (II) coordination compounds of substituted biguanides. Part IV. Inorganica chimica acta. 1990 15;174(2):257-62.

[38]. Goodgame DM, Hitchman MA, Lippert B. Ligating properties of platinum (II) ions in mixed-metal (Pt2M) trimers (M= copper (II), nickel (II), cobalt (II), iron (II)). Inorganic Chemistry. 1986;25(13):2191-4.

[39]. Bhadbhade M, Srinivas D. Erratum to document cited in CA119 (26): 285036b. Inorg. Chem. 1993;32:2458.

[40]. Symons MC. Chemical and Biological Aspects of Electron Spin Resonance, Van Nostrand Reinhold.

[41]. Raman N, Chandrasekar T. Metallonucleases encompassing curcumin, 2-aminobenzothiazole and o-phenylenediamine: a search for new metallonucleases. Inorganic and Nano-Metal Chemistry. 2021 ; 13:1-3.

[42]. El-Tabl AS, Imam SM. New copper (II) complexes produced by the template reaction of acetoacetic-2-pyridylamide and amino-aliphatic alcohols. Transition Metal Chemistry. 1997;22(3):259-62.

[43]. Bano N, Rauf MA, Owais M, Shakir M. Pharmacologically bio-relevant N-functionalized homo-binuclear macrocyclic complexes: Synthesis, spectral studies, biological screening, HSA binding, and molecular docking. Inorganic and Nano-Metal Chemistry. 2019 2;49(12):413-30.

[44]. El-Tabl A, Abou-Sekkina M. Preparation and thermophysical properties of new cobalt (II), nickel (II) and copper (II) complexes. Polish Journal of Chemistry. 1999;73(12):1937-45.

[45]. Ispir E, Toroğlu S, Kayraldız A. Syntheses, characterization, antimicrobial and genotoxic activities of new Schiff bases and their complexes. Transition metal chemistry. 2008;33(8):953-60.